Development and validation of a finite deformation fibre kinking model for crushing of composites

(article starts on next page)

Development and validation of a finite deformation fibre kinking model for crushing of composites

Sérgio Costa [a,*], Martin Fagerström [b], Robin Olsson [a]

[a] RISE SICOMP AB, Box 104, SE-431 22 Mölndal, Sweden
[b] Chalmers University of Technology, Department of Industrial and Materials Science, SE-412 96 Gothenburg, Sweden

ARTICLE INFO

ABSTRACT

A mesoscale model for fibre kinking onset and growth in a three-dimensional framework is developed and validated against experimental results obtained in-house as well as from the literature. The model formulation is based on fibre kinking theory i.e. the initially misaligned fibres rotate due to compressive loading and nonlinear shear behaviour. Furthermore, the physically-based response is computed in a novel and efficient way using finite deformation theory.

The model validation starts by correlating the numerical results against compression tests of specimens with a known misalignment. The results show good agreement of stiffness and strength for two specimens with low and high misalignment. Fibre kinking growth is validated by simulating the crushing of a flat coupon with the fibres oriented to the load direction. The numerical results show very good agreement with experiments in terms of crash morphology and load response.

1. Introduction

In the last decade, stricter emission regulations were imposed in the automotive industry forcing them to reduce emissions. One possibility being explored is to use alternatives to fossil fuels such as electrically powered cars. In parallel with the transition to electric cars, reducing the vehicle weight is also an excellent opportunity being pursued since vehicle weight contributes to approximately 75% of the energy consumption [1]. Lighter cars will lower CO2 emissions as well as provide higher range for electric cars.

Composite materials offer excellent weight saving potential due to their high stiffness and strength to weight ratio [1]. However, to introduce composites in the automotive industry, where the design is driven by numerical simulation, reliable numerical models are necessary. Crash-worthiness is crucial to car design, but when it comes to design of crash parts in composites, there is a lack of reliable Finite Element (FE) models, especially for the longitudinal crushing. Therefore, there is a very strong need to develop and validate FE models for crash situations.

The crash behaviour of composite structures is crucial for automotive designers but is also of interest for designers of e.g. trains and aircraft. A crash is a structural event of a structure under dynamic compression, involving gross deformations, post-buckling and material failure in compression and locally often also in tension. In contrast, crushing describes quasi-static or dynamic compression of the material

beyond its elastic limit, which involves large strains and eventual fragmentation. Thus, material models for crushing are vital for any crash analysis. Experimentally the crush behaviour of the material may be tested by preventing bending or buckling of the specimen during compressive loading [2].

The failure mechanism that can absorb the most energy during crash is kink-band formation [2], which is predominant for longitudinal compression loading [3]. Failure by kinking initiation has been extensively investigated experimentally for uniaxial loading [3,4] as well as for kinking under biaxial loading [5]. On the other hand, kinking propagation has been significantly less studied even though the latter is the most important for energy absorption [6]. Overall, despite numerous publications on fibre kinking [7] there is still a lack of validation of mesoscale models applied in crash. Several models have been proposed, varying from analytical [8,9] to FE based micromechanical [10–12] and more recently to mesoscale/ply level models [13–16] aimed for FE crash analysis. Often, the micro mechanical models are used for comparison with mesoscale models [17]. Despite high variability of models available in the literature, there is no evidence of validation of fibre kinking models in an FE framework during damage growth under longitudinal compression. For crash simulations of automotive components all the microscale models are impractical since they are very cumbersome computationally. Furthermore, the predictive

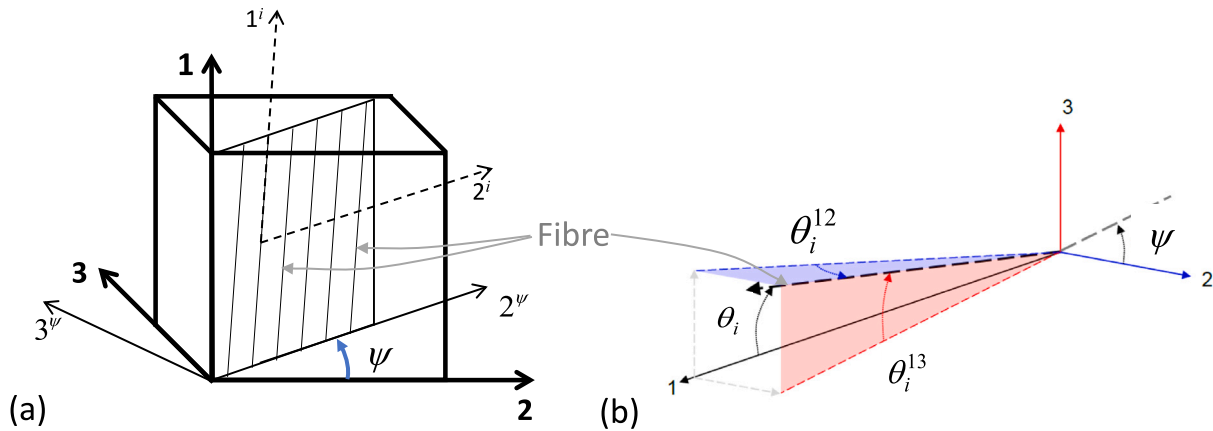**Fig. 1.** Illustration of: (a) 3D kink-band plane resulting from in-plane and out-of-plane misalignment [18]; (b) Definition of initial fibre misalignment.
Source: Adapted from Ref. [19].

capability of kinking models available in the literature has not yet been verified in crash simulations in FE.

The first widely accepted analytical expression for fibre kinking dates from the work of Argon [20] and later Budiansky [21]. This work has been extended to consider nonlinear shear behaviour [8] and both are referred to as Fibre Kinking Theory (FKT). Non-perfectly straight fibres rotating under an applied compressive load induce a degradation of the matrix stiffness. This degradation eases the rotation of the fibres in a positive feedback process, which eventually leads to kink-band formation. The influence of fibre misalignment on the compressive strength was investigated by Wisnom [22] and further investigated by Wilhelmsson et al. [4]. Their work shows that small areas with high fibre waviness may not affect the kinking response as much as bigger areas with smaller average misalignment. On the matrix side, an accurate shear response is fundamental for accurate kinking predictions [23]. Furthermore, Davidson and Waas [24] show that fibre kinking is dictated by the interaction between matrix non-linearity and initial fibre misalignment.

Pinho et al. [18] included the influence of 3D stress states on fibre kinking initiation. By assuming that during kink-band formation the fibres rotate consistently in the same direction forming planes of kinked fibres, a kink-band plane can be defined based on the stress state. Pinho's model shows good strength predictions in correlations with experiments [25] but no assessment on crash predictions has been made. The possibility of failure by instability, rather than by matrix cracking is also introduced in [18]. For kinking propagation, Continuum Damage Mechanics (CDM) with linear softening behaviour is typically used [18,26]. However, since linear softening laws require measurement of the compressive strain energy release rate, which is a highly scattered value [27], they are not suitable to model kink-band propagation. Furthermore, the initial misalignment does not influence the stiffness and more importantly, the severity of the load drop has no correlation with the initial fibre misalignment. These advanced features can usually be captured only by computationally expensive micro-mechanical models [28].

More recently, two fibre kinking models have been proposed that represent a significant departure from the traditional CDM approach. One model was developed by Gutkin, Costa and Olsson [29]. This model was later implemented in Abaqus/Explicit as a VUMAT with two newly developed mesh objectivity approaches [30]. Another model was developed and validated by Bergan et al. [14,31]. One drawback present in the formulation of both of the forementioned models is the need for iterative methods to obtain the kinking response.

In the present model the nonlinear shear behaviour is modelled as a pressure-dependent damage evolution process, which contrasts with the plasticity-based approach by Bergan et al. [14,31]. The pressure

dependence follows from [32], accounting for friction within the microcracks that form during damage development. The frictional effects have a significant influence on the resulting model response, especially under multi-axial stress states. Finally, in the present model, shearing (and thereby rotation) of the fibres comes as a natural output from the model, without the need for any iterations. Being able to avoid iterations within the constitutive relations is beneficial as it leads to a considerable increase in computational efficiency. This increased efficiency is key as the intended application is crashworthiness predictions of engineering structures. The authors believe that besides the gains in efficiency, this approach also adds additional robustness that facilitates the simulation of crash.

The present model is validated against specimens with detailed measurement of the fibre waviness subjected to pure compression loading. The novelty in terms of validation is the crash simulation of a unidirectional (UD) specimen with Non-Crimp-Fabric (NCF) material. It is also demonstrated that the model can handle the post peak response by validating against in-house experiments. The model shows a very robust behaviour, due to its formulation, and the results correlate very well with experiments. Due to the high efficiency, robustness and accuracy of the present model, this work is a major contribution towards simulation of kinking initiation and growth in composite structures.

2. Model description

2.1. Linear elastic behaviour

In engineering composites, the fibres are not perfectly straight. In the present model this imperfection is accounted by an initial misalignment, θ_i. Contrary to typical bilinear models for fibre kinking that assume linear elastic behaviour before the kink-band formation, the current model takes in consideration the fibre misalignment and continuous fibre rotation since loading is applied. To properly allow for finite rotations and deformations, the model is (similarly to [31]) formulated in a large-strain setting where the underlying constitutive assumption relates the second Piola–Kirchhoff stress **S** to the Green–Lagrange strain **E**.

2.2. Initial assumptions and the kink-band plane

We consider that kinking occurs within a transversely isotropic ply, or within the transversely isotropic fibre bundles of an NCF material. During the formation of a kink-band the fibres rotate consistently in the same direction forming the kink-band plane, ψ, as in Ref. [18], see Fig. 1(a). It is considered that the fibres rotate from the very beginning of load introduction. The initial misalignment is defined with two components, one in-plane and one out-of-plane, Fig. 1(b).

Furthermore, the model also takes into account the misalignment of wavy fibres, which is better represented by both positive ($+\theta_i$) and negative ($-\theta_i$) values along the fibres. Thus, to determine the fibre rotation under load it is necessary to consider the solution branch that will cause the largest rotation under the given load, i.e.:

$$\theta_i = \sqrt{\left(\theta_i^{12}\right)^2 + \left(\theta_i^{13}\right)^2} \cdot sign(S_{12}^{\psi}) \tag{1}$$

where S_{12}^{ψ} is the second Piola–Kirchhoff shear stress in the kinking plane. The orientation of the kink-band plane is determined according to the angle between in-plane and out-of-plane waviness as follows:

$$\psi = \tan^{-1}(\theta_i^{13}/\theta_i^{12}). \tag{2}$$

It worth to mention that this approach should yield good results for situations dominated by compressive loading, such as the studied examples, but may not be entirely accurate for more complex stress states. In case the orientation of the initial misalignment is unknown, one should determine a value θ_i that yields the compressive strength of the material [30].

2.3. Formulation of the model

The model formulation follows finite deformation considering the Green–Lagrange (G–L) strain, $\mathbf{E}$, as deformation measure defined as:

$$\mathbf{E} = \frac{1}{2}(\mathbf{F}^T\mathbf{F} - \mathbf{I}) \tag{3}$$

where $\mathbf{F}$ is the deformation gradient and $\mathbf{I}$ is the second order identity tensor. Once the kink-band plane is known, the G–L strain tensor components can be transformed from the global coordinate system to the kink-band plane, ψ. The transformation is (on matrix form) given by:

$$\mathbf{E}^{\psi} = \mathbf{T}_{\psi}\mathbf{E}\mathbf{T}_{\psi}^T \tag{4}$$

where $\mathbf{T}_{\psi}$ is the transformation matrix for a rotation around the 1-axis with an angle ψ. The aim is to model the nonlinear shear response in the material frame, therefore, the strain tensor components need to be further transformed into the 'misaligned' frame as:

$$\mathbf{E}^{\psi,i} = \mathbf{T}_i\mathbf{E}^{\psi}\mathbf{T}_i^T \tag{5}$$

where $\mathbf{T}_i$ is the transformation matrix for rotation with an angle θ_i (around the 3^{ψ}-axis). The constitutive response in the material coordinate system, written in the full form and Voigt notation, is then given by Eq. (6), which is in Box I:

Notice that only the constitutive relation for $S_{12}^{\psi,i}$ is modified from Hooke's law. This modification accounts for the nonlinearity of composites in shear. The proposed way to model that nonlinearity is by combining damage and friction. The damage variable d represents the growth of microcracks between the fibres and S^{fric} is the friction shear stress acting on the crack surfaces [32].

Both fibre kinking onset and growth are very sensitive to the matrix behaviour in shear. Therefore, capturing accurately the shear response is necessary to predict fibre kinking. Combining damage with friction [32] is an efficient way to account for the high nonlinearity, the significant inelastic deformations and the pressure dependency of the shear response. Thus, the shear response on the kink-band plane is modelled by this approach. The remaining components of the stress–strain relationship in the misaligned frame are considered linear elastic but could easily be modified if necessary. The damage, driven by the in-plane shear deformation in the kinking plane $E_{12}^{\psi,i}$, is given as:

$$d = \frac{(2E_{12}^{\psi,i})^p - (\gamma_0)^p}{(\gamma_f)^p - (\gamma_0)^p} \tag{7}$$

where γ_0 and γ_f are the strains at damage initiation and at full decohesion, respectively. The exponent p is used to obtain a closer agreement with the experimental shear stress–strain curve, as shown in Fig. 2. The
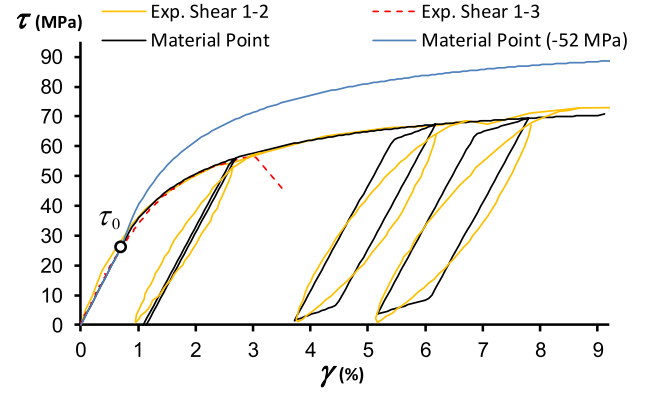

Fig. 2. Shear stress–strain curves from experiments together with model calibration and additional combination of transverse pressure, 40% Yc.

friction shear stress is obtained using a Coulomb sliding criterion in order to account for the stick/slip behaviour as proposed by [32]. Thus, the friction contribution for the sliding case is given by:

$$S^{fric} = -sign(E_{12}^{\psi,i}) \cdot \mu(S_{22}^{\psi,i} - p_o) \tag{8}$$

where μ represents the internal friction coefficient of the material, $S_{22}^{\psi,i}$ is assumed to be the stress influencing the opening/closing of the microcracks and p_o is a calibration parameter representing the internal pressure as suggested by [32]. The shear contact stiffness governing the stick behaviour is assumed to be equal to the in-plane shear modulus, G_{12}.

Note that the shear response of the current model assumes transverse isotropy, i.e. the in-plane and transverse shear responses are modelled by the same curve, which is supported by the experimental data in Fig. 2. The premature final failure of the out-of-plane shear, τ_{13}, is considered to be due to an inter-laminar failure and is therefore not included in the current ply-based model. The model captures well the aforementioned mechanisms of the shear response, as supported by the good match between the model and the experiments, Fig. 2. The influence of pressure on the shear response was validated in Ref. [33].

The components of the second Piola–Kirchoff stress tensor expressed in a coordinate system aligned with the ψ-plane, $\mathbf{S}^{\psi}$ is then found as:

$$\mathbf{S}^{\psi} = \mathbf{T}_i^T \mathbf{S}^{i,\psi} \mathbf{T}_i \tag{9}$$

Finally, for obtaining the global response, the stress tensor needs to be expressed in the global frame according to:

$$\mathbf{S} = \mathbf{T}_{\psi}^T \mathbf{S}^{\psi} \mathbf{T}_{\psi} \tag{10}$$

Given the deformation gradient, $\mathbf{F}$, the Cauchy stress is finally obtained as:

$$\sigma = \mathbf{F}\mathbf{S}\mathbf{F}^{\mathbf{T}} \det(\mathbf{F})^{-1} \tag{11}$$

The present formulation is active until the fibres reach a lock-up angle of about 41 degrees. The influence in the crash response of the fibre lock-up angle, θ_{LU}, is also investigated in the current work. The fibre lock-up occurs when the fibres are in contact and can no longer rotate. Mechanisms, experimental observations and models for fibre lock-up have been reviewed e.g. by [34]. Usually the fibres break in bending and rotate as "rigid rods" prior to lock-up, but they may also break in shear due to axial compression of the fibres after lock-up. Eventually the lock-up is followed by fragmentation where the broken fibre pieces fall apart as a dust or small crumbs. In the present computational model the fragmentation is modelled by element deletion. Since the deletion occurs for a highly compressed element already a long way into the softening regime, retarding the erosion of the element slightly does not cause remarkable changes in the results.

$$
\begin{bmatrix} S^{\psi,i}_{11} \\ S^{\psi,i}_{22} \\ S^{\psi,i}_{33} \\ S^{\psi,i}_{12} \\ S^{\psi,i}_{23} \\ S^{\psi,i}_{13} \end{bmatrix} = \frac{1}{\Delta}
\begin{bmatrix}
E_1(1-v_{23}v_{32}) & E_1(v_{21}-v_{31}v_{23}) & E_1(v_{31}-v_{21}v_{32}) & 0 & 0 & 0 \\
symm & E_2(1-v_{13}v_{31}) & E_2(v_{32}-v_{12}v_{31}) & 0 & 0 & 0 \\
symm & symm & E_3(1-v_{12}v_{21}) & 0 & 0 & 0 \\
0 & 0 & 0 & \Delta(1-d)G_{12} & 0 & 0 \\
0 & 0 & 0 & 0 & \Delta G_{23} & 0 \\
0 & 0 & 0 & 0 & 0 & \Delta G_{13}
\end{bmatrix}
\begin{bmatrix} E^{\psi,i}_{11} \\ E^{\psi,i}_{22} \\ E^{\psi,i}_{33} \\ 2E^{\psi,i}_{12} \\ 2E^{\psi,i}_{23} \\ 2E^{\psi,i}_{13} \end{bmatrix}
+ \begin{bmatrix} 0 \\ 0 \\ 0 \\ dS^{fric} \\ 0 \\ 0 \end{bmatrix}
\tag{6}
$$

where $\Delta = 1 - v_{12}v_{21} - v_{23}v_{32} - v_{13}v_{31} - 2v_{21}v_{32}v_{13}$

Box I.

Table 1
Mechanical properties of HTS45/LY556 NCF composite.

Elastic properties		
Moduli (GPa)		Poisson's ratios
$E_1 = 136$	$G_{12} = 4.4$	$v_{12} = 0.28$
$E_2 = 9.2$	$G_{23} = 3.0$	$v_{32} = 0.43$
$E_3 = 7.7$	$G_{31} = 3.7$	$v_{13} = v_{12}$
Strength properties (MPa)	Initial misalignment	Damage
$\tau_0 = 23$	$\theta_i^{12} = 2.5°$	$p = -0.6$
	$\theta_i^{13} = 2.5°$	$\gamma_f = 0.6$
Friction properties		
Internal pressure (MPa)		Coefficient of friction
$p_0 = 60$		$\mu = 0.4$

From this point onwards an isotropic degradation is activated followed by element removal. This is further discussed in the Element removal section (Section 2.5). To summarize the model, the algorithm for the complete constitutive model is shown in Fig. 3.

2.4. Material properties

The material properties of the uni-weave carbon/epoxy NCF composite, used in all application cases in this paper, were taken from Refs. [35,36]. The full set of data used in the present model is summarized in Table 1. The damage parameters are p (used to calibrated from the shear stress–strain curve), γ_0 is the shear strain at onset of damage ($\gamma_0 = \tau_0/G_{12}$) and γ_f is the shear strain at final decohesion. The friction parameters are the coefficient of friction on the micro-crack surfaces μ, and the internal pressure p_0. Note the lack of strength properties except the onset of nonlinearity in the shear response, τ_0. This value is defined visually from the beginning of shear nonlinearity in the shear response and is only used to obtain γ_0. The in-plane and out-of-plane fibre misalignments are represented by θ_i^{12} and θ_i^{13} respectively. They are used in the cases where the fibre waviness is unknown, such as in the crash specimen. Note that a higher θ_i^{13} could be used to represent a higher out-of-plane waviness observed in NCF materials [37].

2.5. Element removal

The strategy to delete distorted elements uses an scalar isotropic damage, d^{iso}, that degrades all stress components equally, similar to Ref. [32]. A fibre lock-up angle of 41 degrees was used as suggested in Ref. [6], i.e. when fibre lock-up is reached, the scalar isotropic damage is activated. The evolution of this damage is driven by the additional fibre rotation and subsequently all stress components are smoothly degraded to zero. The isotropic damage variable evolves linearly reaching one within a 3 degrees interval, see Fig. 4. When the isotropic damage reaches one, the element is no longer carrying any load and it is removed.

The calculation of the fibre rotation assumes affine rotation of the fibres. Thus, this valuable output of the model, can be obtained more
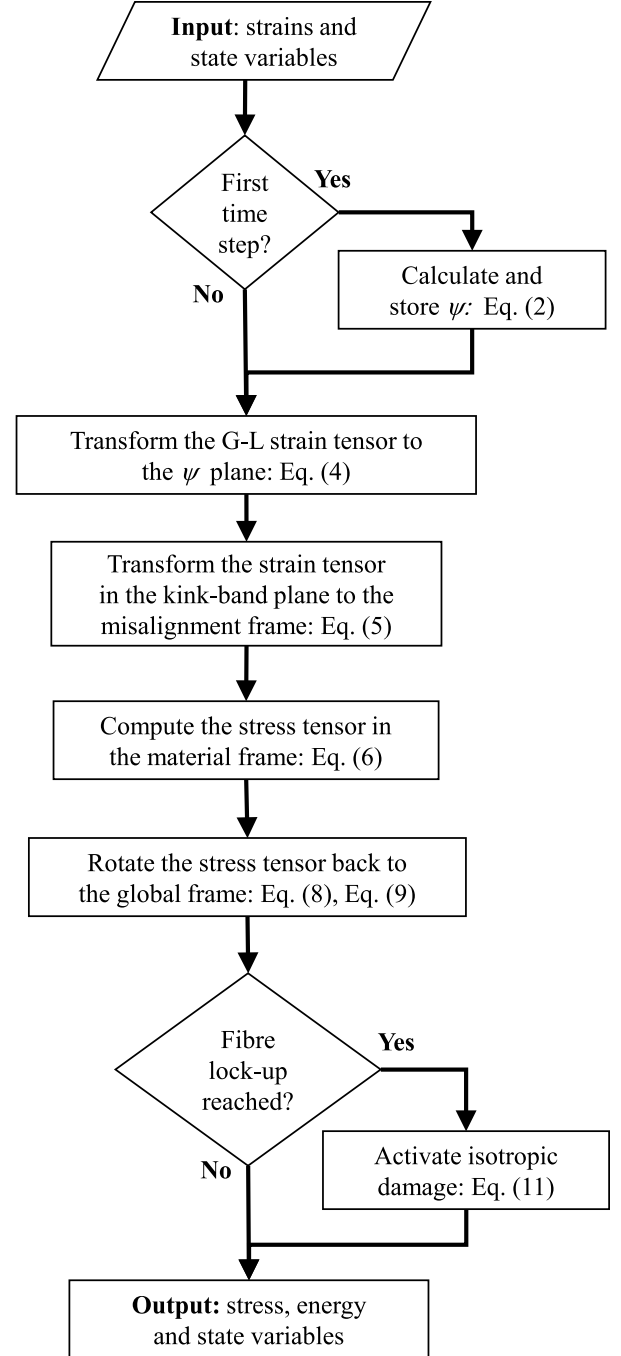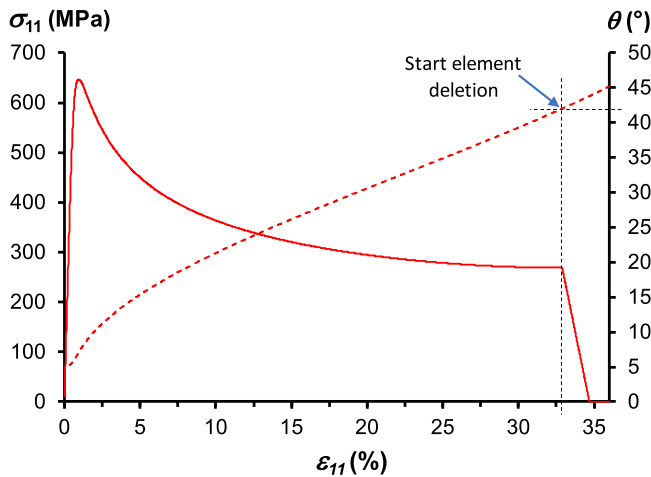
Fig. 3. Algorithm of the present model.

Fig. 4. Element deletion driven by fibre rotation for a uniaxial loading situation with 3.5 degrees initial misalignment.

Fig. 5. Single element predictions of kinking stress and fibre rotation for 2°, 3.5°, 5° of initial misalignment.

efficiently than other approaches that require iterative methods, [14, 32]. In case the element distorts excessively before fibres lock-up, a criterion based on the determinant of the deformation gradient (similar to in Ref. [13]), is also introduced for additional robustness. The full conditions are:

Start d^{iso} when: $\theta > 41°$

Remove element when: $\begin{Bmatrix} d^{iso} = 1 \\ \det(\mathbf{F}) < 0.3 \\ \det(\mathbf{F}) > 1.7 \end{Bmatrix}$ (12)

where $\mathbf{F}$ is the deformation gradient. The $\det(\mathbf{F})$ represents the ratio between the deformed and the undeformed volume. Tan et al. [38] used $\det(\mathbf{F}) < 0.8$ or $\det(\mathbf{F}) > 1.6$ as the criteria for element deletion. The robustness of the proposed formulation allows for higher element distortions before the element needs to be removed. The complete stress–strain response is shown in Fig. 4. Note that the starting point of element deletion corresponds to approximately 33% strain for the pure uniaxial stress case.

3. Model validation

3.1. Uniaxial response

The current model was developed with focus on crash simulations, where the damage growth dominates the response. However, the physically-based nature of the model, i.e. predicting the kinking response based fibre rotation and shear non-linearity makes the model very suitable also for strength predictions. In Fig. 5, the kinking stress, σ_{11}, is plotted on the left axis and the fibre rotation, θ, on the right axis. The first observation in Fig. 5 is perhaps the high sensitivity of the strength to the fibre misalignment, where the strength is significantly higher for lower initial misalignment. For $\theta_i = 2°$, the fibres start by rotating at a lower rate followed by a sudden rotation when the peak load is reached. Considering that the fibres start to rotate from the very beginning results in higher stiffness for lower initial misalignments. The load drop, as consequence of shear instability, is more abrupt (unstable) for lower initial misalignments.

3.2. Validation of stiffness and strength

The peak load is predicted as a result of shear instability due to fibre rotation and nonlinear shear. In fact, the whole response follows the same mechanism. Therefore, by validating the known parts of the response, and assuming the same mechanism prevails throughout
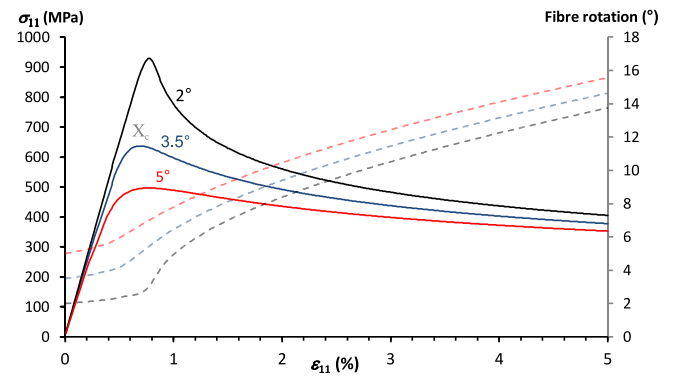
kinking formation, one can extrapolate the validity to the remaining model until another failure mechanism occurs. Thus, in this section the model is validated against experiments for the stiffness and strength.

When it comes to mesoscale models, the typical approach is to calculate the fibre misalignment as an initial imperfection from the material properties [18,26]. This approach would not be suitable to validate the model since we would back calculate an imperfection based on known values of strength. Instead, using as input the detailed fibre waviness data, allows for validation of the model assumptions. Furthermore, using the actual misalignment values answers an important question: how much of θ_i is related to actual fibre waviness and how much is related to imperfections in the material, such as voids or stitching yarns.

Simulations of the stress–strain behaviour of the compression tests have also been presented by Wilhelmsson et al. [4]. Their approach to predict fibre kinking initiation is based on the FE equilibrium rather than on FKT. The fibre misalignments are associated with the elements coordinate system, which shear (rotate) under compressive load. In their approach, fibre kinking seems to be predicted by instability due to element rotation rather than by instability in the material. The nonlinear shear response is identical to the current model and to previous work in Refs. [33,36]. Their approach has not been investigated for kink-band propagation nor for crash simulations.

The initial misalignments are provided by Wilhelmsson et al. [39] from micrographs of specimens, using the developed High Resolution Misalignment Analysis (HRMA). The representation of the spatial misalignment for a High Waviness specimen (identified as B1) is shown in the contour plot, Fig. 6(a). Note that Fig. 6 shows the cross-section of the laminate where the out-of-plane (direction-3) of the laminate is pointing upwards and the in-plane (direction-2) is normal to the figure.

The raw data from the literature is shown in Fig. 6(a), all the other figures are obtained from processing this data. An algorithm is used to filter all the white pixels that correspond to areas where it was not possible to obtain measurements. Another algorithm is used here to remove the unrealistic spikes in the measurements. This filter removes the sudden peak values and smooths out the waviness according to the surrounding values. The result of both filters is shown in Fig. 6(b). Finally, in order to have a larger element size, i.e. one element per ply, the values of 16 measurements were averaged to one, see Fig. 6(c). Note that the element size is identical for all simulations. This is intentional since the model lacks an internal length scale and therefore would experience a pathological mesh sensitivity during the damage evolution. To regularize the model and to capture the right energy absorption during the localization of deformation, we therefore keep an element size which corresponds to an approximate value of the kink-band width. An extension to a mesh-objective formulation is however possible in several ways, following e.g. the work in Refs. [14,30], but has been excluded for brevity in the current paper.
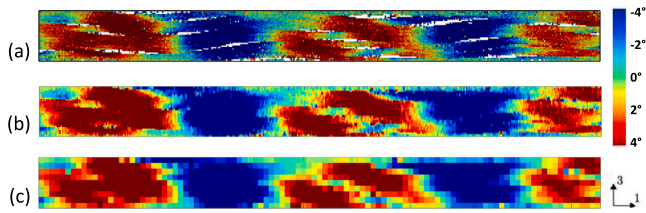
Fig. 6. Representative spatial distributions of fibre misalignment angles for specimen B1. (a) Adapted from Wilhelmsson [39]. (b) The white pixels and unphysical spikes of (a) are smoothed out. (c) Applied as an average of 4 × 4 pixels of (b).

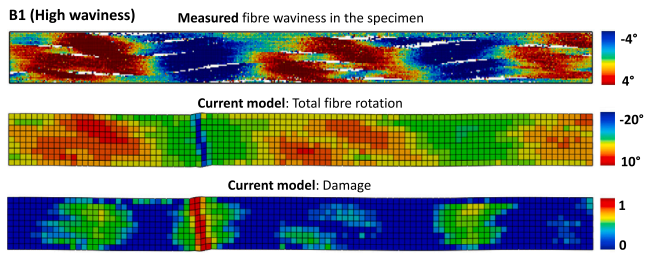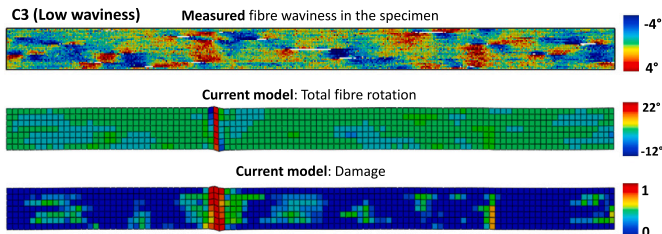**Fig. 7.** Measured waviness, fibre rotation and damage given by the model at peak load for specimen B1.

Fig. 8. Measured waviness, fibre rotation and damage given by the model at peak load for specimen C3.

Fig. 9. Model vs. experimental response.

The out-of-plane fibre misalignments were used to create an FE model in Abaqus/Explicit 2016. A single row of elements is used in the 2-direction since the in-plane misalignment is considered to have less influence on the response. To avoid possible buckling in the direction-2, a symmetric BC is applied in this direction. A fixed support is applied on the left side and simple displacement in direction-1 is applied on the right side of the specimen. The model was created using a developed python script that transforms the data from the fibre misalignments into material properties with a unique θ_i per element. The element size was 0.22 mm, which corresponds to 4 times more than the spatial resolution of the measured misalignments (55 μm).

The original spatial distributions of fibre misalignments and the results in terms of damage and fibre rotation are shown in Fig. 7. The deformation localizes into a kink-band, where there is a clear kink-band through the whole thickness, with the elements shearing in the same direction as the fibres represented by them. The damage follows the same pattern as the fibre rotation, although it is useful to identify other critical areas that were otherwise unnoticeable from the fibre rotation plot.

Another specimen, this time a Low Waviness specimen, identified as C3 in [39] was also correlated for increasing confidence in the results, Fig. 8. The figure shows the representation of the measured spatial misalignment and the results of the present model in terms of fibre rotation and damage. Again, the results show a clear kink-band through the thickness.

As a final comparison between both models and the experiments, the FE response of specimens B1 and C3 is compared with the measured
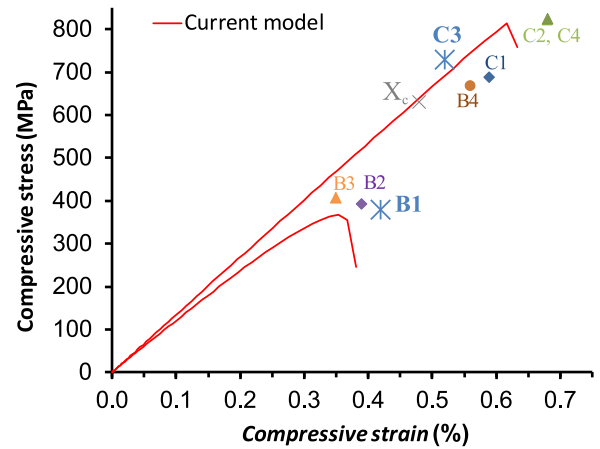
strength and strain at failure [39], see Fig. 9. The first observation is that specimens with lower initial waviness have higher stiffness and significantly higher strength. The proposed model correlates well with the experiments in terms of stiffness, strength and fairly well with the strain at failure. It is worth to point out that typical bilinear CDM will not account for any stiffness variations since their response is considered linear-elastic prior to failure [40]. In bilinear laws the θ_i only influences the failure criteria, i.e. the peak stress, ignoring thus an important aspect of kinking formation.

From the above results, one can conclude that for the current model the waviness of the fibres is overall well represented by θ_i. This shows that θ_i is mainly related to actual fibre waviness and that there is no need for additional adjustments to include possible voids (at least not for the current NCF material). This answers the previous question and is an important observation since up to now it was considered to include all sorts of imperfections.

3.3. Validation of the crushing response

After validating the ability of the model to predict the kink-band formation, in this section the model is challenged in a situation dominated by kink-band growth. An arrow shaped specimen is crushed longitudinally, resulting, at the microscopic level, in bands of fibres rotating in different directions. The material system is the same as in the previous validation, the UD NCF material characterized in Ref. [2]. The simple design of the specimen helps to maximize kinking formation as well as to identify and correlate the crush mechanisms with the simulation. The fractography shows that 80% of the cross-section is failing by kinking, although there is still 20% of the specimen that seems to fail by delamination and splaying (i.e. out-of-plane bending of plies), which absorbs considerably less energy [2]. At the current stage delaminations were not included in the model since: (i) the test shows that most of the crash response is due to fibre kinking growth; (ii) including delaminations could mask the constitutive response of the model making it more difficult to know whether the response is due to kinking growth or due to delaminations; (iii) the transverse response of the model needs to be further developed to capture more accurately the out-of-plane shear stresses, responsible for delamination onset and growth.

The geometry of the specimen and its supports are shown in Fig. 10. This setup is identical to the setup used for model validation of shear and transverse crushing in a previous paper by Costa et al. [33]. We refer to that paper for further details about the choice of specimen and analysis methodology. Here we mention the main aspects of the experimental and numerical setup.
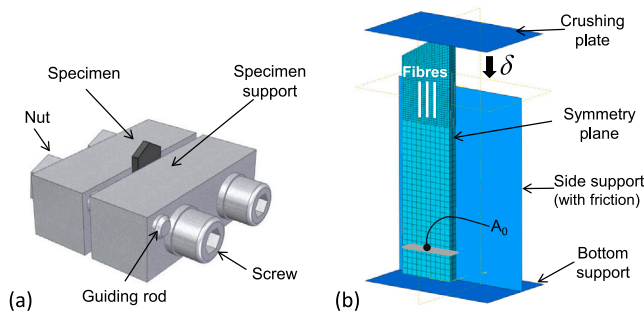
Fig. 10. Representative geometry of the crush specimen: (a) Specimen support and boundary conditions of the test set-up (adapted from Ref. [3]); (b) FE set-up.
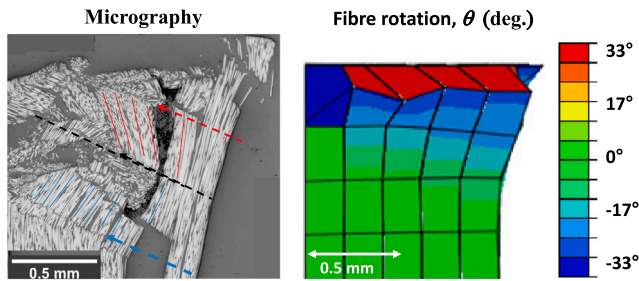

Fig. 11. Comparison between micrograph of an initially crushed specimen and the FE results.

The composite specimens used were $[0°]_{10}$ HTS45/LY556 carbon uniweave/epoxy fabricated by resin transfer moulding, with properties

given in Table 1. The experiments were performed under quasi-static conditions. For comparison, virtual crush specimens were created in ABAQUS/Explicit 2016 with one element per ply in the crushing zone. The loading was introduced by applying a vertical displacement, of a rigid crushing plate. Furthermore, in order to have faster simulations, a linear elastic material and a bigger element size was used in the bottom of the specimens, i.e. away from the crushing zone. A value of $\psi = 45°$ was assumed (i.e. $\theta_i^{13} = \theta_i^{12}$) since the ratio of θ_i^{13} and θ_i^{12} is unknown.

The first results of the crash simulation are correlated with the micrograph of an interrupted experiment done in Ref. [41], Fig. 11.

Overall, the morphology of the partially crushed specimen is well captured by the model. Two main bands of kinking fibres can be identified, the first rotating anti-clockwise and the second clockwise. Also, two rows of elements are rotating substantially more than the surrounding elements. The lateral profile of the specimen also matches well with the simulation. Note that spring back of the specimen will occur when the experiment is interrupted, and the load is removed. This may explain the fact that the progression of damage and kinking extends further down in the experiment than in the simulation, which shows a loaded state.

The final validation is the comparison of the response with experiments. The nominal stresses, expressed as the axial load F divided by the cross-sectional area A_0, are plotted against the crushing length, normalized with the end of the trigger, shown in Fig. 12.

Note that the increasing nominal stress up to the end of the trigger is a direct result of the linearly increasing cross section. Thus, a constant slope in the trigger and a subsequent constant plateau value indicates a constant crush stress, which is the *average* stress during crushing of the material up to fragmentation (element deletion).

In Fig. 12 the predicted response for 3.5° fibre misalignment is in very good agreement with the experiment and very similar to the response for 6.0° misalignment. This is in line with experimental results in Ref. [41], where a similar crush stress and energy absorption was obtained for all off-axis angles up to 15.0°. The spikes in the predicted
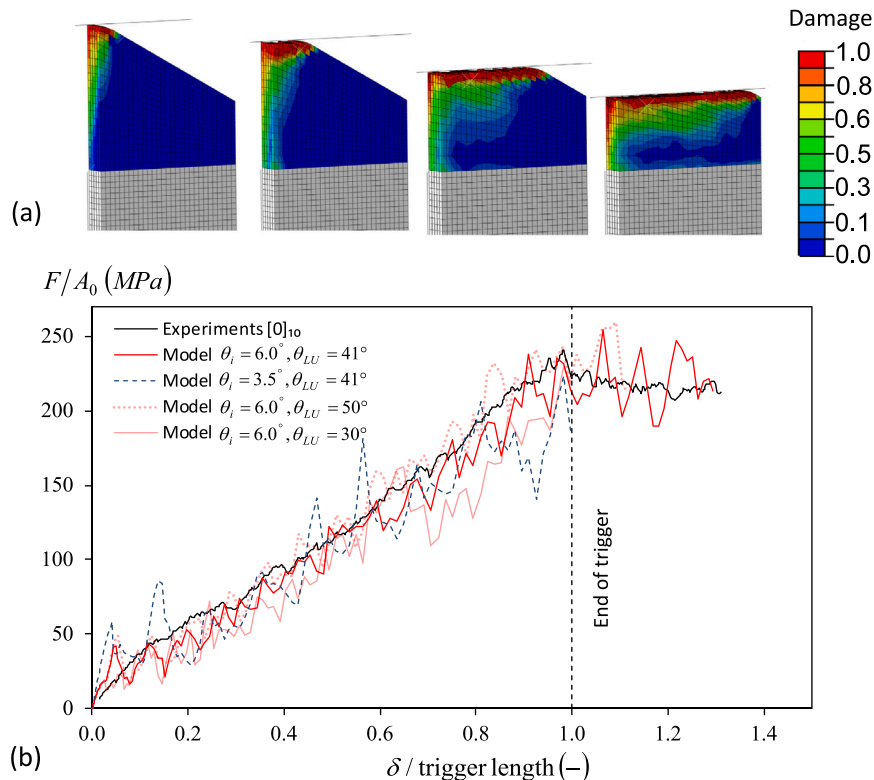

Fig. 12. Crushing response for the $[0°]_{10}$ crush specimen: (a) Damage at 4 different stages; (b) Experimental vs. numerical response for different fibre misalignments and lock-up angles.

response curves reflect individual elements reaching the peak stress of the compressive stress–strain curves. As evident from Fig. 5 the compressive strength and the amplitude of such spikes will increase with decreasing fibre misalignment, although the average crush stress is not significantly affected. Also note that the influence of the assumed fibre lock-up is relatively small.

4. Conclusions and outlook

A new 3D model formulation for fibre kinking was presented and validated against two sets of experiments. The kink-band formation is governed by instability due to shear nonlinearity as in FKT. The shear nonlinearity is modelled efficiently by combining damage and friction [32]. Pressure dependency of the shear response and inelastic deformations are also included. The constitutive response is expressed in the material frame, making it easy to include other damage mechanisms, such as matrix cracking. The current model, compared to the most recently developed models, excels on the following:

1. The kinking response is obtained without iterative methods, thus speeding up greatly the simulation.
2. The model shows robustness and is capable to handle the post peak response. This was demonstrated and validated by simulating crash against in-house experiments.
3. The model does not require compressive intralaminar toughness measurement, reducing thus characterization efforts.
4. The FE implementation is very straightforward and the modifications to the constitutive behaviour can be easily introduced.
5. Large deformation theory is included in the model formation.

The validation of the model for stiffness and strength shows good correlation with the experiments. The influence of initial misalignments on the stiffness is well captured by the model. The strength defined at the onset of unstable fibre rotation is well predicted for two specimens with low and high fibre waviness. In addition, the crushing response shows very good agreement with experimental results in terms of morphology in the crushing zone, as well as in the load response. The ability of the present mesoscale model to capture fibre rotation is of great importance for accurate crash simulations. It allows to account for accurate interaction with matrix cracks and delaminations in the adjacent plies [42,43]. The present model for fibre kinking of composites, shows accuracy and robustness, Therefore, it is a valuable tool for designing composite applications driven by strength and energy absorption.

The influence of strain rate is not considered in the current model. Unpublished experimental data from a related project considering the same material system as the present paper indicates moderate rate effects during kinking, as an increase of the displacement rate from 0.002 m/s to 7 m/s reduced the crush stress of a 0°/90° laminate by less than 20%. Efforts to include rate effects are, however, ongoing and will be presented in future models from our research group.

For future work it is important to develop and validate the model in scenarios that involve kink-band formation and growth under substantial transverse and shear loads, i.e modelling and validation of multiaxial stress state. Furthermore, investigating the influence of delaminations as well as to introduce an efficient mesh objective formulation would also be beneficial.

CRediT authorship contribution statement

Sérgio Costa: Conceptualization, Methodology, Software, Validation, Visualization, Writing - original draft. **Martin Fagerström:** Conceptualization, Methodology, Supervision, Writing - review & editing. **Robin Olsson:** Conceptualization, Supervision, Writing - review & editing.

Declaration of competing interest

The authors declare that they have no known competing financial interests or personal relationships that could have appeared to influence the work reported in this paper.

References

[1] C. Park, C. Kan, W. Hollowell, S. Hill, Investigation of opportunities for lightweight vehicles using advanced plastics and composites, Tech. Rep. DOT HS 811 692, National Highway Safety Administration, USA, 2012.

[2] T. Bru, P. Waldenström, R. Gutkin, R. Olsson, G.M. Vyas, Development of a test method for evaluating the crushing behaviour of unidirectional laminates, J. Compos. Mater. 51 (29) (2017) 4041–4051.

[3] A.M. Waas, C.R. Schultheisz, Compressive failure of composites, part ii: Experimental studies, Prog. Aerosp. Sci. 78 (1996) 32–43.

[4] D. Wilhelmsson, R. Talreja, R. Gutkin, L. Asp, Compressive strength assessment of fibre composites based on a defect severity model, Compos. Sci. Technol. 181 (2019) 107685.

[5] F. Edgren, L.E. Asp, R. Joffe, Failure of ncf composites subjected to combined compression and shear loading, Compos. Sci. Technol. 66 (15) (2006) 2865–2877.

[6] S.P.H. Skovsgaard, H.M. Jensen, Steady-state kink band propagation in layered materials, J. Appl. Mech. 85 (6) (2018) 061005.

[7] O. Allix, N. Feld, E. Baranger, J.-M. Guimard, C. Ha-Minh, The compressive behaviour of composites including fiber kinking: modelling across the scales, Meccanica 49 (11) (2014) 2571–2586.

[8] B. Budiansky, N. Fleck, Compressive failure of fibre composites, J. Mech. Phys. Solids 41 (1) (1993) 183–211.

[9] S. Basu, M.W. Anthony, D. Ambur, Compressive failure of fiber composites under multi-axial loading, J. Mech. Phys. Solids 54 (2006) 611–634.

[10] S. Pimenta, R. Gutkin, S. Pinho, P. Robinson, A micromechanical model for kink-band formation: Part i — experimental study and numerical modelling, Compos. Sci. Technol. 69 (7) (2009) 948–955.

[11] Q. Sun, G. Zhou, H. Guo, Z. Meng, Z. Chen, H. Liu, H. Kang, X. Su, Failure mechanisms of cross-ply carbon fiber reinforced polymer laminates under longitudinal compression with experimental and computational analyses, Composites B 167 (2019) 147–160.

[12] M. Bishara, R. Rolfes, O. Allix, Revealing complex aspects of compressive failure of polymer composites – part i: Fiber kinking at microscale, Compos. Struct. 169 (2017) 105–115.

[13] W. Tan, B.G. Falzon, Modelling the nonlinear behaviour and fracture process of as4/pekk thermoplastic composite under shear loading, Compos. Sci. Technol. 126 (2016) 60–77.

[14] A.C. Bergan, F.A. Leone, A continuum damage mechanics model to predict kink-band propagation using deformation gradient tensor decomposition, in: American Society for Composites 31st Technical Conference, 2016.

[15] R. Larsson, R. Gutkin, M.S. Rouhi, Damage growth and strain localization in compressive loaded fiber reinforced composites, Mech. Mater. 127 (2018) 77–90.

[16] M. Bishara, M. Vogler, R. Rolfes, Revealing complex aspects of compressive failure of polymer composites – part ii: Failure interactions in multidirectional laminates and validation, Compos. Struct. 169 (2017) 116–128, In Honor of Prof. Leissa.

[17] M. Herraez, A. Bergan, C. González, Modeling fiber kinking at the microscale and mesoscale, Tech. Rep. TP–2018–220105, NASA, 2018.

[18] S.T. Pinho, L. Iannucci, P. Robinson, Physically based failure models and criteria for laminated fibre-reinforced composites with emphasis on fibre kinking: Part I: Development, Composites A 185 (2006) 774–785.

[19] A.C. Bergan, A three-dimensional mesoscale model for in-plane and out-of-plane fiber kinking, in: AIAA SciTech 2019 Forum, San Diego, CA, United States, 7-11 January 2019.

[20] A.S. Argon, Fracture of Composites (Treatise on Materials Science and Technology), NY Acad Press, 1972.

[21] B. Budiansky, Micromechanics, Comput. Struct. 16 (1) (1983) 3–12.

[22] M.R. Wisnom, Analysis of shear instability in compression due to fibre waviness, J. Reinf. Plast. Compos. 12 (11) (1993) 1171–1189.

[23] S.-Y. Hsu, T. Vogler, S. Kyriakides, Compressive strength predictions for fiber composites, J. Appl. Mech. 21 (1998) 1–18.

[24] P. Davidson, A. M. Waas, Mechanics of Kinking in Fiber-Reinforced Composites Under Compressive Loading, NY Acad Press, 2014.

[25] A.S. Kaddour, M.J. Hinton, Maturity of 3D failure criteria for fibre-reinforced composites: Comparison between theories and experiments: Part B of WWFE-II, J. Compos. Mater. 47 (6–7) (2013) 925–966.

[26] P. Maimí, P. Camanho, J. Mayugo, C. Dávila, A continuum damage model for composite laminates: Part i – constitutive model, Mech. Mater. 39 (10) (2007) 897–908.

[27] D. Svensson, K. Alfredsson, U. Stigh, N. Jansson, Measurement of cohesive law for kink-band formation in unidirectional composite, Eng. Fract. Mech. 151 (2016) 1–10.

[28] P. Prabhakar, A.M. Waas, Interaction between kinking and splitting in the compressive failure of unidirectional fiber reinforced laminated composites, Compos. Struct. 98 (2013) 85–92.

[29] R. Gutkin, S. Costa, R. Olsson, A physically based model for kink-band growth and longitudinal crushing of composites under 3D stress states accounting for friction, Compos. Sci. Technol. 135 (2016) 39–45.

[30] S. Costa, R. Gutkin, R. Olsson, Mesh objective implementation of a fibre kinking model for damage growth with friction, Compos. Struct. 168 (2017) 384–391.

[31] A.C. Bergan, M. Herráez, C. González, C.S. Lopes, A constitutive model for fiber kinking: Formulation, finite element implementation, and verification, Composites A (2019) 105682.

[32] R. Gutkin, S.T. Pinho, Combining damage and friction to model compressive damage growth in fibre-reinforced composites, J. Compos. Mater. 49 (20) (2015) 2483–2495.

[33] S. Costa, T. Bru, R. Olsson, A. Portugal, Improvement and validation of a physically based model for the shear and transverse crushing of orthotropic composites, J. Compos. Mater. 53 (12) (2019) 1681–1696.

[34] R. Olsson, Fibre lock-up and other mechanisms at large fibre rotations, and their effect on axial compression of composites, in: European Conference on Composite Materials. Paper 3.11(2)-08, 2018.

[35] T. Bru, P. Hellström, R. Gutkin, D. Ramantani, G. Peterson, Characterisation of the mechanical and fracture properties of a uni-weave carbon fibre/epoxy non-crimp fabric composite, Data Brief 6 (2016) 680–695.

[36] T. Bru, R. Olsson, R. Gutkin, G.M. Vyas, Use of the iosipescu test for the identification of shear damage evolution laws of an orthotropic composite, Compos. Struct. 174 (2017) 319–328.

[37] D. Wilhelmsson, R. Gutkin, F. Edgren, L. Asp, An experimental study of fibre waviness and its effects on compressive properties of unidirectional ncf composites, Composites A 107 (2018) 665–674.

[38] W. Tan, B.G. Falzon, M. Price, Predicting the crushing behaviour of composite material using high-fidelity finite element modelling, Int. J. Crashworthiness 20 (1) (2015) 60–77.

[39] D. Wilhelmsson, L. Asp, A high resolution method for characterisation of fibre misalignment angles in composites, Compos. Sci. Technol. 165 (2018) 214–221.

[40] S.T. Pinho, L. Iannucci, P. Robinson, Physically based failure models and criteria for laminated fibre-reinforced composites with emphasis on fibre kinking. Part II: Fe implementation, Composites A 37 (2006) 766–777.

[41] T. Bru, R. Olsson, G.M. Vyas, et al., Validation of a novel model for the compressive response of FRP: experiments with different fibre orientations, in: Proceedings of ICCM-21 Conference, Xi'an, China, 20–25 August, 2017.

[42] N. Zobeiry, R. Vaziri, A. Poursartip, Characterization of strain-softening behavior and failure mechanisms of composites under tension and compression, Composites A 68 (2015) 29–41.

[43] C. Sola, B. Castanié, L. Michel, F. Lachaud, A. Delabie, E. Mermoz, On the role of kinking in the bearing failure of composite laminates, Compos. Struct. 141 (2016) 184–193.